**IMPACT OF TSUNAMI FORCES ON STRUCTURES  
The University of Ottawa Experience****D. Palermo, I. Nistor & T. Al-Faesly**  
*University of Ottawa, Ottawa, Canada***A. Cornett**  
*National Research Council, Ottawa, Canada***ABSTRACT**

Over the past seven years, a comprehensive interdisciplinary research program has been conducted between researchers at the University of Ottawa and at the Canadian Hydraulics Centre (CHC) of the National Research Council of Canada. The objectives of this on-going research program are to identify and quantify forces that are imposed on near-shoreline structures when exposed to tsunami-induced hydraulic bores and to investigate mitigation strategies to dampen these forces. The experimental component of this research program involves two structural models (square and circular) that are tested in the High Discharge Flume at CHC. The structural models are instrumented to record base shear force-, base overturning moment-, pressure-, acceleration-, lateral displacement- and bore depth-time histories continually during testing. Impact loading resulting from wood debris of different sizes and located at pre-determined distances from the structural models is also studied. Furthermore, this research program aims to review tsunami-induced forces on structures prescribed by recent design documents.

*Keywords: Tsunami; hydrodynamic loading; debris impact; building performance; and design guidelines.*

## 1. INTRODUCTION

During the last decade, three significant tsunamis (Indian Ocean 2004, Chile 2010, and Japan 2011) have impacted coastal regions resulting in catastrophic human and economic losses. These events have illustrated that infrastructure located near coastlines in tsunami inundation zones is vulnerable to significant damage from rapidly advancing tsunami surges and bores. The tsunamis, while devastating, have provided the engineering community with unique opportunities to learn about the response of inland structures that are typically not designed to withstand the forces imposed by the resulting tsunami waves. They have provided an avenue to investigate the performance of non-engineered and engineered structures, and various building materials. In addition, beyond lateral loading, reconnaissance trips to the affected areas have brought to light other important structural mechanisms that need to be considered in the design of tsunami-resilient structures. These include, but are not limited to: debris impact loading and debris damming as a consequence of floating debris that is transported by the advancing tsunami flow; uplift forces associated with the rapidly rising water level; overturning of structures due to lateral loading; and scouring of foundations. The following provides specific details of the three major tsunamis mentioned above.

### 1.1 2004 Indian Ocean Tsunami

The 26 December 2004 Indian Ocean tsunami marks a significant historical event. Researchers and engineers became more attentive to tsunami hazard as a result of the significant damage to many coastal communities and the massive human casualties that was experienced across the Indian Ocean. Prior to this event, with the exception of a limited number of shelter-type structures, tsunamis were not considered in the design of inland structures located within inundation zones. It was also a “wake-up” call for other regions of the world located near subduction zones, particularly those located around the “Pacific Ring of Fire”. The Indian Ocean tsunami was triggered by a 9.1 magnitude (Richter scale) earthquake along the northwestern coast of the Indonesian island of Sumatra. The earthquake focal depth for this event was approximately 30 km. The main fault rupture zone was approximately 90 km wide and 1200 km long. A maximum tsunami run-up of approximately 51 m was observed in Indonesia (NGDC, 2012). From a structural engineering perspective, significant lessons were learnt, such as the types of loading that are generated during a tsunami event and the vulnerability of non-engineered structures. Fig. 1 (a) highlights the global damage suffered by non-engineered residential structures due to the advancing tsunami flow. Figs. 1 (b) and (c) depict the large objects that were transported by the tsunami, which resulted in significant impact loading on structural components. Fig. 1 (d) captures the uplift and displacement of concrete dock slabs due to the rapidly rising tsunami.



(a)



(b)



(c)



(d)

Figure 1. Effects of 2004 Indian Ocean tsunami on structures (Saatcioglu et al., 2006a, 2006b): a) global damage to non-engineered concrete residential structure in Phuket Island, Thailand; b) debris impact and damming in Banda Aceh, Indonesia; c) debris impact from large vessels in Banda Aceh, Indonesia; and d) uplift of concrete slabs in Khao Lak, Thailand.

## 1.2 The 2010 Tsunami in Chile

*On 27 March 2010, an 8.8 magnitude (Richter scale) earthquake struck offshore Chile, along the boundary between the Nazca and South American Plates. The earthquake focal depth for this event was approximately 30 km and was situated offshore Bio-Bio. Specifically, the epicenter was located 95 km NW of Chillan. The rupture causing the earthquake had a width of over 100 km and a length of approximately 500 km and was parallel to the Chilean central coastline. The tsunami was first observed in Valparaiso 30 minutes after the earthquake (Dunbar et al. 2010). The highest wave height noted during a field survey by Lagos et al. (2010) was 11.2 m in the town of Constitución, while 8.6 m high waves were measured in Dichato and Tome. Fritz et al. (2011) noted that the tsunami reached a*

localized runup of 29 m on a coastal bluff at Constitución. The maximum inundation distance of approximately 1032 m was observed in Playa Purema. While many coastal communities suffered widespread damage, the number of casualties attributed to the tsunami was low. According to the International Tsunami Information Center, approximately 124 deaths were attributed to the tsunami. This was a direct result of two factors. First, Chile had experienced a major tsunami in 1960, which remains engrained in the memory of the local population. The 1960 event was triggered by a 9.5 magnitude earthquake, and approximately 1000 deaths were directly attributed to the tsunami. The highest wave height was 25 m at Isla Mocha (Dunbar et al. 2010). For the 2010 tsunami, in general, those living along the coast immediately searched for higher ground upon experiencing the ground shaking caused by the earthquake. Second, the central coastline of Chile is in close proximity to higher ground providing a natural vertical evacuation. Fig. 2 illustrates damage sustained by residential dwellings in the coastal community of Pelluhue. The photos reveal that the homes were fully inundated by the tsunami.



Figure 2. Effects of 2010 Chile tsunami on residential structures in Pelluhue (Palermo et al., 2013): a) global damage to two storey-structure; b) punching failure of second storey masonry infill walls; c) damage to masonry infill walls and loss of load bearing elements at first storey level; and d) destruction of lower level columns.

The residential structure in Fig. 2 (a) suffered punching failure of the infill masonry walls at the second storey level and failure of the lower level bearing elements. Timber columns were used at the lower level as temporary vertical supports. The residence in Fig. 2 (c) also sustained complete failure of the lower level columns, and temporary timber columns were used to support the upper level.

Fig. 3 (a) shows signage that was evident in Tome to direct people away from the inundation area and to safe higher ground, while Fig. 3 (b) is a photo depicting the higher ground that is within the coastal region that is typical of many communities in Chile.



Figure 3. Evacuation: a) tsunami evacuation route directions in Tome, Chile (Palermo et al., 2013); and b) higher ground in Pelluhue, Chile

### 1.3 2011 Japan Tsunami

A powerful earthquake of magnitude 9.0 (Richer scale) occurred at a depth of 30 km under the Pacific Ocean, near the northeast coast of Japan. The epicenter of the earthquake was located approximately 129 km east of Sendai, Honshu, and the subsequent tsunami arrived on the northeastern coast of Japan approximately 15 minutes thereafter, leaving little warning time for many villages and communities. Local run-up heights of up to 48 m were estimated (Chock et al. 2012). This event was responsible for approximately 15 867 deaths, 6 109 injuries, and 2 909 people missing. The Japanese Cabinet Office estimated direct losses of more than \$309 billion due to damage to housing, roads, utilities, and businesses, making it the most expensive natural disaster on record. The destruction caused by this tsunami was surprising. Japan is a leading country when it comes to protection against tsunami; however, the tsunami waves displaced, overtopped and destroyed large structures, such as seawalls, which were initially constructed to mitigate the impact of tsunami waves on local communities. The designs of these structures were based on historical tsunamis and were not necessarily sufficient considering probabilistic-based tsunami events. Fig. 4 illustrates the effects of the tsunami, including breaching and overtopping of large concrete sea walls, floating vessels, overturning of a concrete building, and punching failure of a reinforced concrete wall panel.



(a)



(b)



(c)



(d)

Figure 4. Effects of 2011 Japan tsunami on structures (Nistor, 2012): a) breaching and overtopping of concrete sea walls in Taro; b) impact loading from large vessel in Otsuchi; c) overturning of reinforced concrete apartment building in Onagawa; and d) punching failure of reinforced concrete walls in Onagawa

## 2. EXPERIMENTAL PROGRAM

In response to the observed structural damage of near-shoreline structures in tsunami inundation zones, an experimental testing program was developed between the University of Ottawa and the Canadian Hydraulics Centre (CHC) of the Natural Research Council (NRC) of Canada. The motivation for this research originated from findings of a field reconnaissance mission to Thailand, Indonesia and Sri Lanka following the 2004 Indian Ocean tsunami (Nistor et al., 2006). One of the main objectives of the program is to identify the forces imposed on structures from turbulent

hydraulic bores that are representative of the tsunami-induced bores generated in many of the areas affected by tsunami inundation during the 2004 Indian Ocean, 2010 Chile and 2011 Japan tsunamis. This was achieved by partitioning a pre-existing open channel high discharge flume at CHC and installing a swinging hinged gate. The gate was installed near the upstream end of a 1.3 m wide by 7.3 m long channel, and was capable of impounding water in the closed position. The gate is able to open rapidly, releasing a turbulent hydraulic bore that travels downstream and impacts structural models (Nouri et al., 2010). This mechanism is similar to a dam-break phenomenon. Chanson (2005) demonstrated that dam-break flows could provide a reasonable simulation of tsunami-induced turbulent hydraulic bores. Fig. 5 is a photo of the high discharge flume with the gate in the open position producing a turbulent hydraulic bore.



Figure 5. Turbulent hydraulic bore generated in the high discharge flume at the Canadian Hydraulics Centre

Fig. 6 provides top and elevation view drawings of the experimental setup wherein the location of the wave gauges used to measure the water depth; the structural models and mitigation walls are labeled. Also shown are the three impounded water levels investigated in this experimental program.

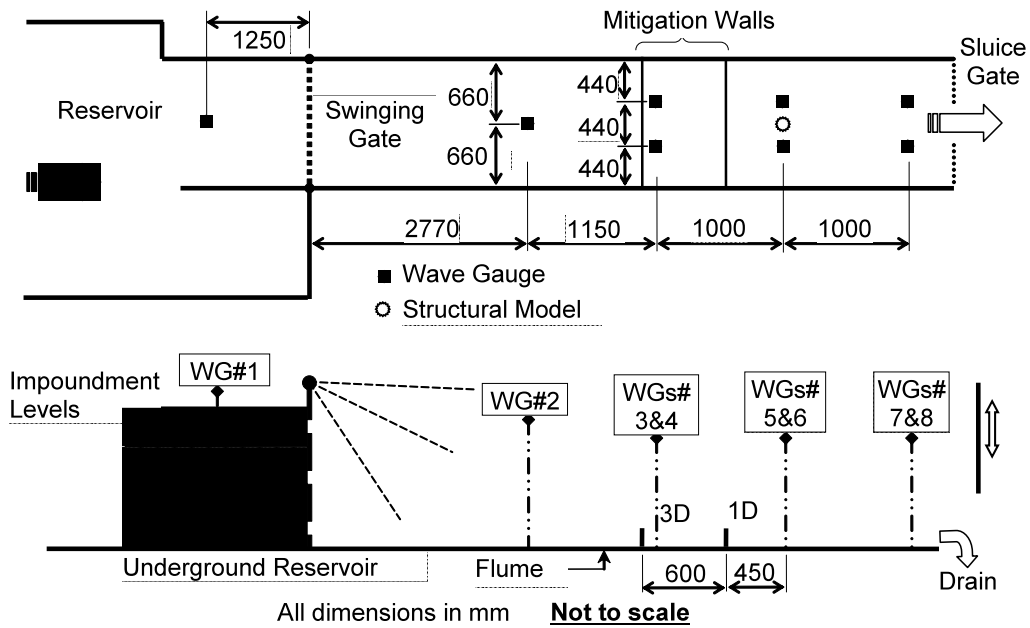


Figure 6. Drawings of experimental setup

Two hollow structural models, square and circular in cross section, were used in this experimental program. The hollow square structural model has 305 mm x 305 mm cross section, measured to the outside of the section. The walls are 6.35 mm thick and consist of acrylic glass sheets. The hollow circular model, also of acrylic material, has an outside diameter of 305 mm with a wall thickness of 9 mm. Photos of the two structural models installed in the flume are shown in Fig. 7.



Figure 7. Hollow square and circular structural models (Al-Faesly et al., 2012)

The structural models were rigidly fastened to a six degree-of-freedom high-frequency dynamometer that, in turn, was fixed to the floor of the flume. The dynamometer was used to record base shear forces and base overturning moments. Ten pressure transducers were arranged vertically on the outer surface of the structural models to record pressures. Nine of the ten transducers were spaced at intervals of 50 mm starting from the flume floor, while the tenth transducer was positioned 20 mm above the flume floor. Pressures on different faces of the structural models were obtained by rotating the models. An accelerometer and a linear variable displacement transducer were placed at the top of the models to record accelerations and displacements in the direction of the flow, respectively. In addition to the instrumentation placed on the models, the flume was fitted with several capacitance water level gauges (Fig. 6) to record the water depth along the flume. All sensor measurements were recorded continuously during testing, at rates up to 1000 samples per second, to obtain time history responses.

A number of parameters and processes have been investigated in this experimental program, including: the water level impounded behind the swinging gate, the initial condition of the flume bed (dry or wet), the shape of the structural model impacted by the hydraulic bores, the response to debris impact, and the performance of upstream mitigation walls intended to reduce the peak forces acting on the structural models.

### **3. EXPERIMENTAL RESULTS**

The experimental results presented herein include bore-depth time histories at the location of the structural model, base shear force-time histories in the direction of the flow recorded for the square structural model, and flow velocity-time histories at the location of the structural model. The bore depth and corresponding velocity provides essential data to evaluate current force expressions used in design documents.

#### **3.1 Bore Depth, Base Shear Force, and Pressures**

Fig. 8 provides typical bore depth-time history responses recorded by the water level gauges placed around the square model and the base shear force-time history recorded by the dynamometer. These results were generated with the 550 mm impounded water level behind the swinging gate in the closed position. The upstream gauges (WG9 and WG10) measured an instantaneous spike in water level followed by a sharp decrease. This spike coincided with the initial impact of the bore front on the structure and was caused by a thin jet of highly aerated water flowing rapidly up the column face. Immediately following the initial impact, some water was reflected upstream while the advancing bore was surging up the front face of the structural model. This led to a second rise in water level followed by a quasi-static flow condition where the water level remained approximately constant with time.

The base shear force-time history shown in Fig. 8 (b) also reveals an initial spike in force, which occurs when the leading edge of the turbulent bore impacts the structural model. Thereafter, there is a

drop in force as the bore rebounds upstream from the upstream face of the model. This is followed by an increase in force as the bore flow accumulates in front of the structure causing a “bulb-like” wake. The latter mechanism leads to the maximum force experienced by the structural model, and has been termed “run-up force” (Palermo et al., 2009) or “transient hydrodynamic force”. The first impact or impulse force (approximately 222 N) was recorded when the water depth at the upstream face of the column (at gauge WG9) was approximately 0.52 m. The run-up force was approximately 264 N, which coincided with a water level of approximately 0.39 m. The force-time history does not suggest the presence of a steady hydrodynamic force; however, between 8 to 10 s, the force was approximately constant and equal to 220 N. The water level recorded at WG9 was approximately 0.36 m during this time period.

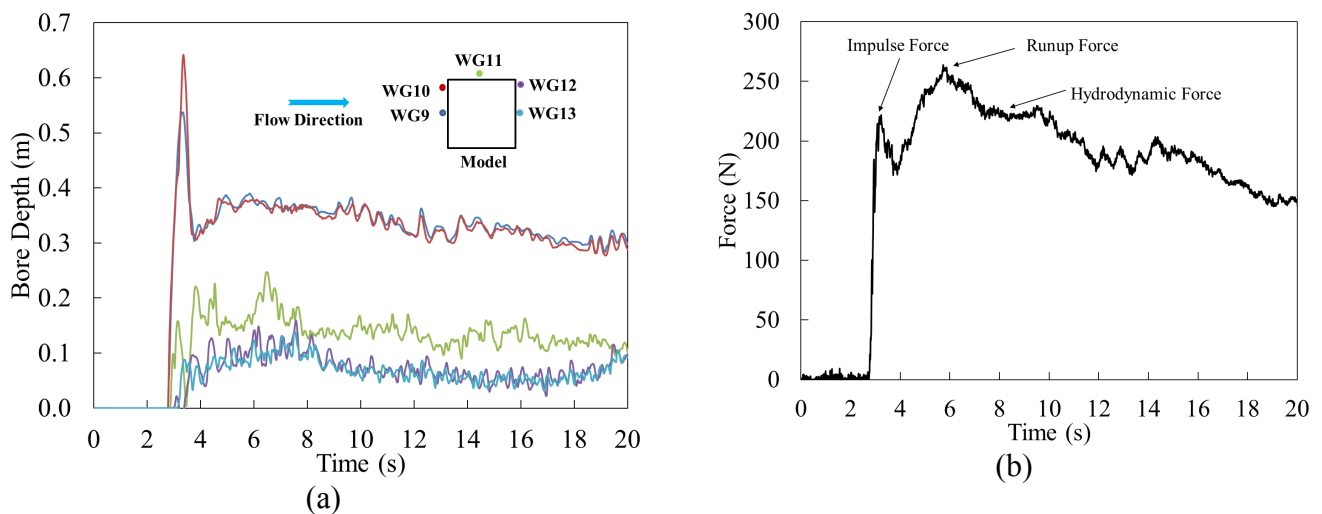


Figure 8. Experiment data for 550 mm impoundment depth: a) bore depth-time histories around the square model; and b) base shear force-time history

Fig. 9 provides still images from a video recording showing the three stages of flow interaction with the square structural model that coincide with the force components identified in Fig. 8 (b). The three stages are: the reflection of the flow from the front face of the square model after the initial impact; the run-up condition as the rebounding water meets with the advancing bore and surges up the model; and the quasi-steady state flow condition.

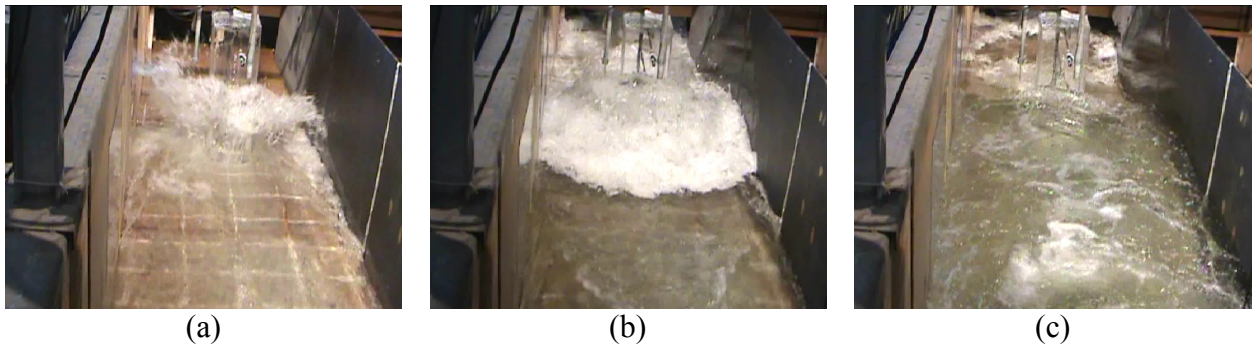


Figure 9. Hydraulic bore-structural model interaction: a) initial impact; b) run-up; and c) quasi-steady flow

Fig. 10 shows the vertical pressure distributions recorded on the upstream face of the square model at three different times during a single flow-structure interaction. The times correspond to the impulse force, run-up force and quasi-steady hydrodynamic force identified in Fig. 8 (b). For all three times, the pressure profiles were consistent with a hydrostatic distribution. Furthermore, it is evident that all pressure transducers, with the exception of the gauge located 450 mm above the flume bottom, which remained above the maximum water level, recorded pressures. Therefore, at all three times during the interaction, the water level on the upstream face of the square model reached approximately 400 mm. This result is inconsistent with the measurements at water level gauge WG9, and suggests that gauge WG9 recorded a higher water level during the initial impact as a result of the water rebounding off the upstream face of the structure. For the run-up and hydrodynamic force conditions, the pressure gauges recorded a slightly higher water level due to the water surging up the front face of the model.

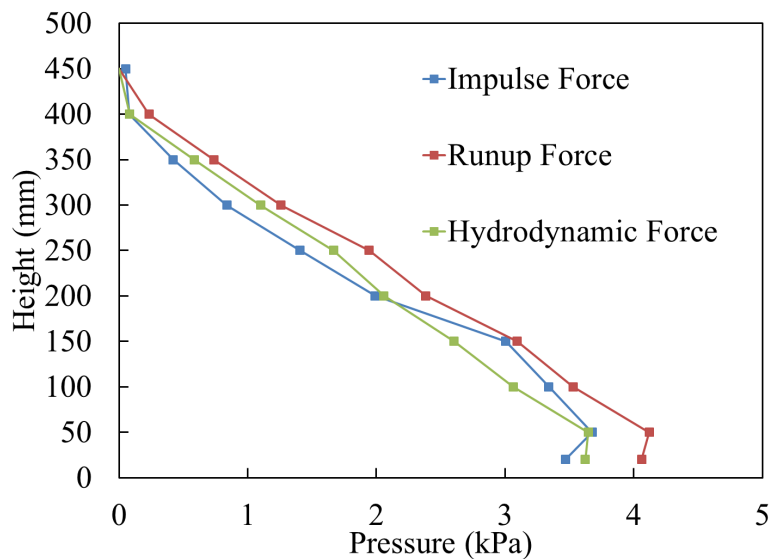


Figure 10. Vertical pressure distributions on the upstream face of the square model

From the hydrostatic pressure profiles of Fig. 10, the individual force components (i.e. impulse, run-up and hydrodynamic) can be evaluated. For each force component, the height of the pressure was assumed to be 400 mm, while the pressures at the base are approximately 3.67 kPa, 4.12 kPa, and 3.65 kPa, for the impulse, run-up, and hydrodynamic forces, respectively. These pressure values corresponded to the transducer readings 50 mm above the base of the structure. This slightly overestimates the pressure at the base of the structure, but offsets the 0 kPa pressures assumed at the 400 mm elevation. Based on these assumptions, the calculated forces were 224 N, 250 N, and 222 N for the impulse, run-up, and hydrodynamic force components, respectively. These are in close agreement with the base shear forces measured by the dynamometer and illustrated in Fig. 8 (b).

The bore depth measured at the location of the structure, without the structure in the flume, is shown in Fig. 11. For the 550 mm impoundment depth, the water reached a maximum elevation of 0.22 m at approximately 13.5 s. This peak water level was sustained for approximately 10 s as water drained from the impoundment. It is interesting to note that the water level on the upstream face of the structure was approximately 0.4 m based on the pressure readings. Therefore, the presence of the structural model causes a local increase in bore depth near the upstream face. In addition, the influence of the width of the flume relative to the width of the structural model may be a contributing factor.

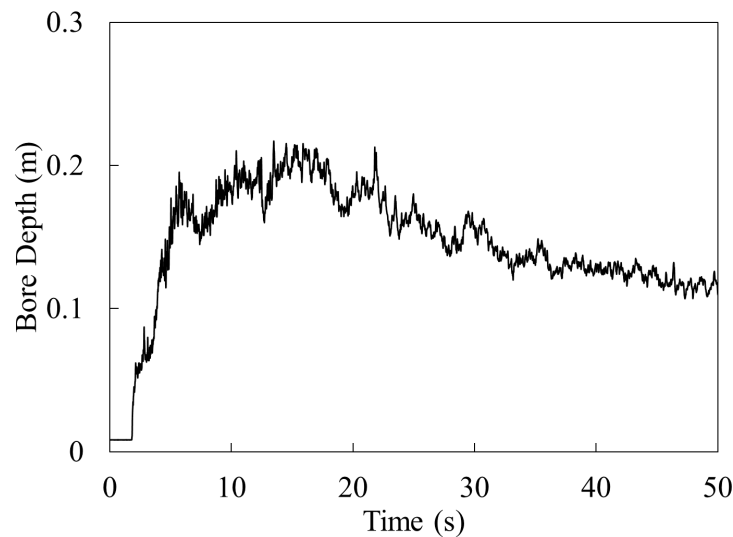


Figure 11. Bore depth-time history in the absence of the structural model

### 3.2 Bore Velocity and Hydrodynamic Forces

The bore velocity-time history corresponding to the measured bore depth-time history in Fig. 11 is shown in Fig. 12. The velocity was measured by seeding the water with 25 mm square paper beads and tracking their position by analysing images recorded by a high-speed video camera positioned above the flow. The video camera, as shown in Fig. 12 (a), was fastened 2.40 m above the floor of the flume at the location of the structure. Two wooden bar markers were arranged horizontally across the

width of the flume, 0.3 m apart from each other and 0.48 m above the floor of the flume. The distance ( $D_w$ ) travelled by the paper, which was captured by the video camera, varied with the water depth and was adjusted according to the geometry shown in Fig. 12 (a). Therefore, using the adjusted distance and the time for the paper to flow between the wooden markers, the bore velocity-time history at the location of the structural models was calculated (see Fig. 12 (b)). Note that this procedure measures the velocity at the surface of the bore.

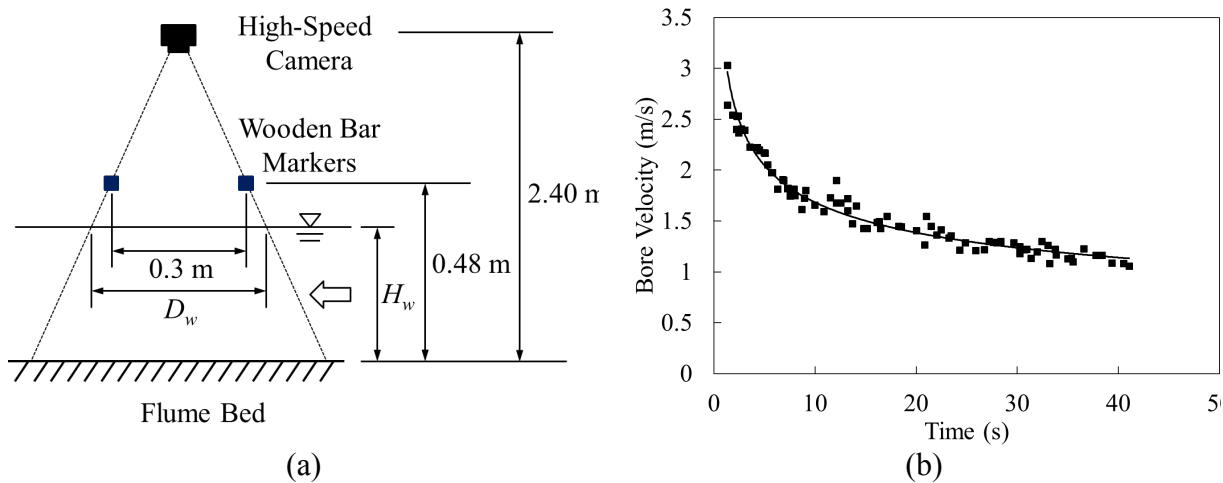


Figure 12. Bore velocity for 550 mm impoundment depth: a) velocity tracking setup; and b) measured bore velocity-time history at the location of the structural model

Fig. 12 clearly demonstrates that the bore front velocity was significantly higher than the velocity during the time period from 10 – 20 s in which the bore depth reached a maximum. The surface velocity near the leading edge of the bore was approximately 3.0 m/s, double the 1.5 m/s velocity that prevailed between 10 – 20 s. The bore depth-time history and corresponding bore velocity-time history were used to calculate the momentum flux (the product of the bore depth and the corresponding velocity squared). This parameter is used to estimate the hydrodynamic forces as provided in Eqn. 2.1 and published in FEMA P646 (2012):

$$Fd=12\rho sCdBhu^2max \quad (2.1)$$

where  $r_s$  is the fluid density, (approximately 990 kg/m<sup>3</sup> for this test program);  $C_d$  is the drag coefficient, assumed equal to 2 for square elements;  $B$  is the width of the element (0.305 m for the square structure); and  $(hu^2)_{max}$  is the maximum momentum flux, which would need to be estimated from the bore depth- and bore velocity-time histories for the site, or obtained by some other means. Fig. 13 (a) provides the calculated momentum flux-time history, while Fig. 13 (b) shows the hydrodynamic force-time history obtained by applying Eqn. 2.1. The base shear force-time history recorded by the dynamometer is included in the figure for comparison. Note that the two force-time histories are offset for clarity.

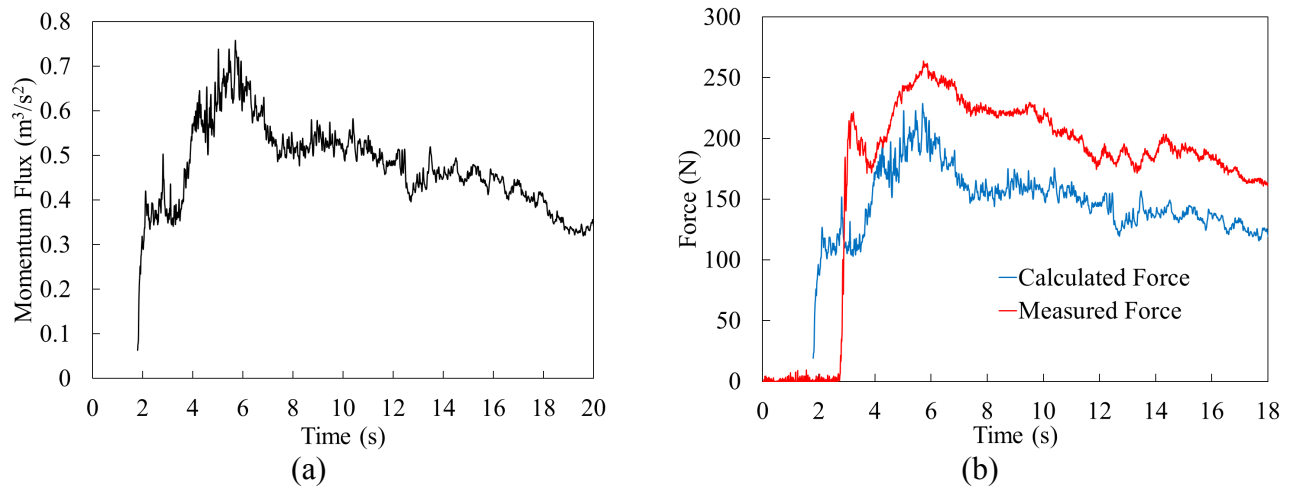


Figure 13. Calculated values for 550 mm impoundment depth: a) momentum flux-time history; and b) base shear force-time histories

The results illustrate that the calculated forces follow the same trends as the measured forces; however, the calculated force under-estimates the maximum force in this case. The peak calculated force was approximately 229 N, while the peak recorded force was 264 N or 15% larger. This difference in peak force may be attributed to a number of sources, such as measurement error, variability between repeated tests, the confining effect of the flume walls, and error in the assumed value for  $C_d$ .

For a site where the bore depth- and bore velocity-time histories are not available, FEMA P646 provides an analytical approach to calculate the maximum momentum flux:

$$hu_{2max} = gR^{2.125} - 0.235zR + 0.11zR^2 \quad (2.2)$$

where  $g$  is the acceleration due to gravity,  $R$  is the design run-up elevation, and  $z$  is the ground elevation at the base of the structure. For the experimental setup presented herein,  $z$  is taken as 0, and Eqn. 2.2 simplifies to:

$$hu_{2max} = gR^{2.125} \quad (2.3)$$

FEMA P646 suggests that the design run-up elevation,  $R$ , be taken as 1.3 times the maximum run-up elevation to account for uncertainties in determining the design run-up. Using a maximum bore depth of 0.22 m from Fig. 11, and applying the 1.3 factor, Eqn. 2.3 predicts a maximum momentum flux of 0.098  $m^3/s^2$ . The corresponding maximum hydrodynamic force using Eqn. 2.1 is 29 N. This result demonstrates that the momentum flux formulation (Eq. 2.2) provided in FEMA P646 may not be applicable for near-zero sloping beaches. Similar findings were obtained for a number of other similar tests conducted by the authors (Al-Faesly et al., 2012). Note that FEMA P646 (2012) indicates that Eq. 2.2 is based on one-dimensional nonlinear shallow water theory for a uniformly sloping beach.

### 3.3 Debris Impact Testing

The field surveys conducted after the 2004 Indian Ocean, 2010 Chile and 2011 Japan tsunamis highlighted the severe impact of debris on structures. As part of this experimental program, debris impact tests were conducted using 3 wood logs of different size and mass: 77 mm x 77 mm x 490 mm (1.09 kg), 77 mm x 77 mm x 916 mm (2.19 kg), and 77 mm x 154 mm x 490 mm (2.26 kg). Fig. 14 (a) shows the setup of a typical debris impact test prior to the opening of the gate, and Fig. 14 (b) captures the impact of the log against the circular structural model. The wooden logs were placed on the floor of the flume at pre-determined distances from the structural model before each test. As the bore advanced downstream from the gate, the flow accelerated and transported the debris, causing it to impact against the structural model.

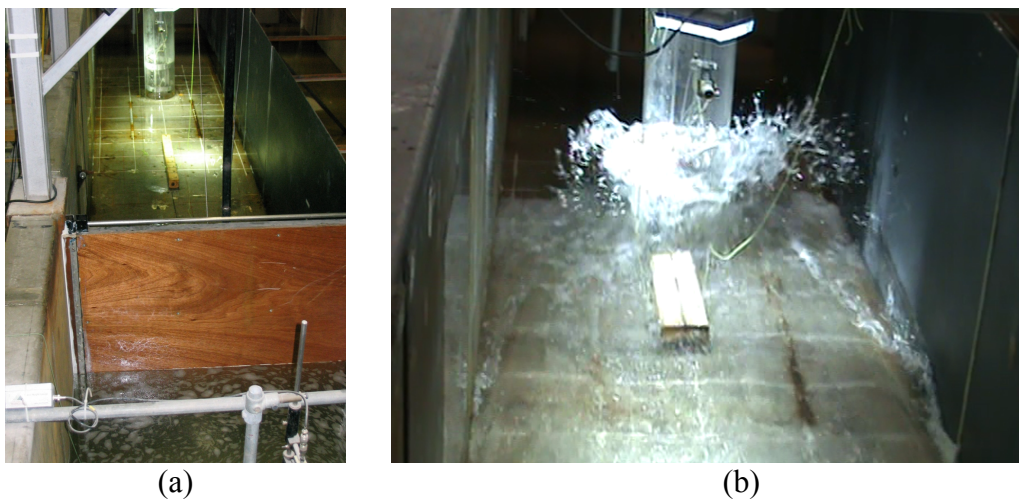
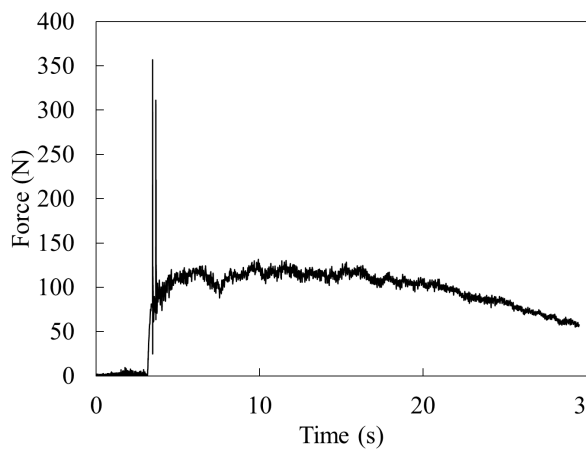


Figure 14. Debris impact testing: a) initial setup; and b) debris impacting circular structural model  
Fig. 15 provides a typical impact test result for the circular structural model. The results correspond to the 1.09 kg wood debris initially located 1.75 m downstream from the swinging gate.

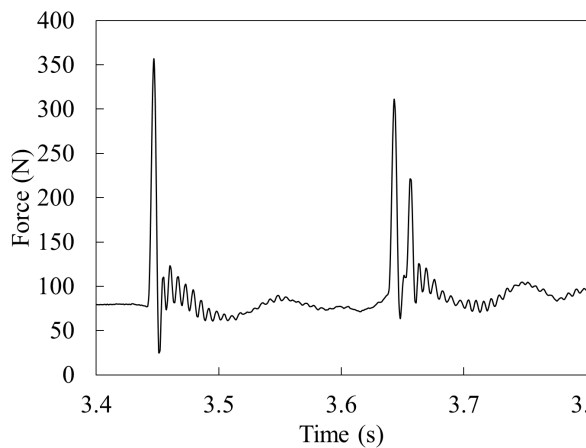
Fig 15 (a) provides the entire base shear force-time history where the spike in force is attributed to the wood log impacting the structural model. The first impact occurs shortly after the bore front reaches the upstream face of the model. The first impact force was approximately 279 N (net of the force imposed by the flow of the water) with a corresponding rise time of 0.005 s. Fig. 15 (c) shows the base shear force-time history between 3 and 4 s where two additional impacts are evident. They occur due to the log rebounding from the structure and then being carried back into the structure by the bore. The second and third net impact forces were approximately 220 N and 144 N, respectively, with rise times of 0.005 s and 0.007 s. Fig. 15 (b) demonstrates that the first impact was a direct longitudinal strike, while the second and third impacts were more of a transverse strike (Fig. 15 (d)). The second and third impact forces were smaller than the first impact force due, in part, to the reduced velocity of the log and the change in orientation from longitudinal to transverse.



(a)



(b)



(c)



(d)

Figure 15. Debris impact test results: a) base shear force-time history; b) orientation of first impact; c) base shear force-time history of subsequent impacts; and d) orientation of subsequent impacts

### 3.4 Flume Bed Condition

Another interesting phenomenon observed during the experiments was the influence of the condition of the flume bed. Fig. 16 compares the base shear force-time histories experienced by the square structural model when subjected to flows generated by the 550 mm impoundment depth. Fig. 16 (a) illustrates the measured response under dry-bed conditions (an initial condition with negligible water on the flume bed), which typically corresponded to the first test of the day. This condition could reasonably represent in-land ground conditions during the arrival of the first tsunami wave. Fig. 16 (b) provides the measured response under wet-bed conditions (an initial condition wherein the flume bottom was covered by a thin film of water), which corresponded to all subsequent tests. This could be representative of the ground conditions for subsequent tsunami waves. The corresponding bore depth-time histories are also superimposed in Fig. 16.

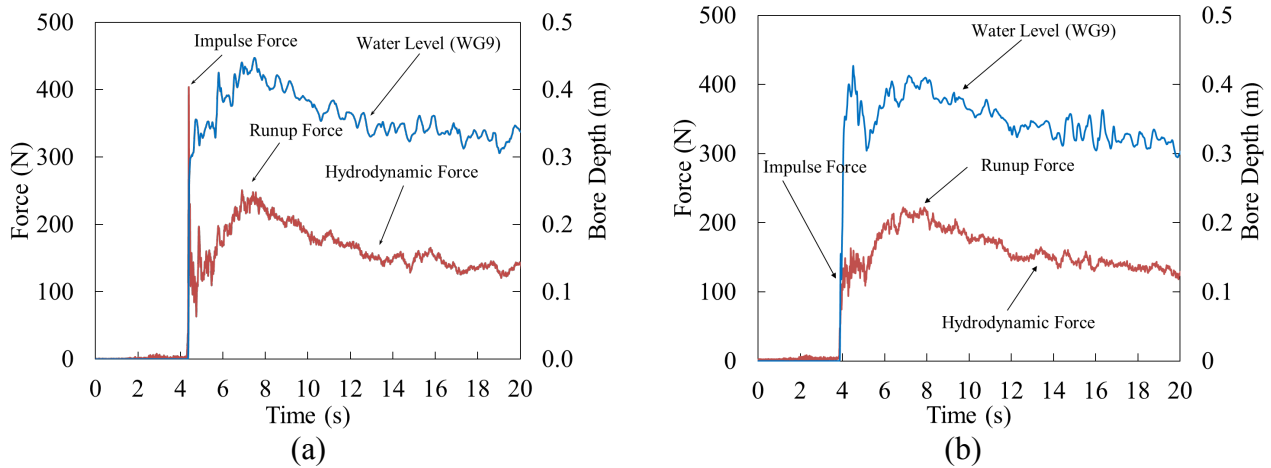


Figure 16. Effect of dry bed vs. wet bed for 550 mm impoundment water level: a) time histories for dry bed; and b) time histories for wet bed

The bore depth-time histories recorded by WG9, located near the upstream face of the structural model, for the wet- and dry-bed conditions are similar. The base shear force-time histories are also similar beyond the initial impulse force. The only notable difference is the initial impulse force. For the dry-bed condition, the initial impulse force was approximately 404 N, while under the wet-bed condition; the initial impulse force was only 134 N. It became evident from observing high-speed video recordings that the leading edge of the bore front was steeper in the case of the dry flume bed, which is attributable to the greater friction generated by the dry-bed surface. This phenomenon resulted in the significantly higher impulse force for the dry-bed condition.

#### 4. CONCLUSIONS

The severe impact of tsunami-induced bores on near-shoreline structures has been well documented by recent events in the Indian Ocean (2004), Chile (2010), and Japan (2011). Based on observations from site visits to these areas, the University of Ottawa in collaboration with the National Research Council of Canada have collaborated to conduct experimental studies to further the knowledge of tsunami loading of near-shore structures. This paper has presented typical findings, from which a number of conclusions are drawn:

1. A dam-break process can be used to generate turbulent hydraulic bores similar to those observed in recent tsunami events.
2. The presence of a structure modifies the bore depth- and bore velocity-time histories around the structure relative to the undisturbed flows in the absence of the model.

3. Three distinct phases of forcing were typically observed during testing: impulse, run-up, and quasi-steady hydrodynamic.
4. For the test results presented herein, the vertical pressure distribution on the upstream face of a square structure can be well approximated as a hydrostatic pressure distribution throughout the flow-structure interaction.
5. Properly assessing the momentum flux is critical to accurately predicting the hydrodynamic force-time history. The analytical solution provided by FEMA P646 to calculate the maximum momentum flux is not applicable for near-zero sloping beaches.
6. Impact testing reveals that single debris objects can generate multiple impact events, with the first impact generating the maximum force.
7. The initial dryness of the flume bed was found to have a strong influence on the magnitude of the initial impulse force, with significantly larger impulse forces recorded under a dry-bed condition.

## REFERENCES

- AL-FAESLY, T., PALERMO, D., NISTOR, I., AND CORNETT, A. (2012). Experimental modeling of extreme hydrodynamic forces on structural elements. *International Journal of Protective Structures (IJPS)*, **3:4**, 477-505.
- CHANSON, H. (2005). Analytical solution of dam break wave with flow resistance. Application to tsunamis. *31<sup>st</sup> International Association for Hydro-Environment Engineering and Research (IAHR) Congress*, 3341-3353.
- CHOCK, G., ROBERTSON, I., KRIEBEL, D., FRANCIS, M., AND NISTOR, I. (2012). Tohoku Japan tsunami of March 11, 2011 – Performance of structures, *American Society of Civil Engineers (ASCE)*, 297 p.
- DUNBAR, P., STROKER, K., AND MCCULLOUGH, H., (2010). Do the 2010 Haiti and Chile earthquakes and tsunamis indicate increasing trends? *Geomatics, Natural Hazards and Risk* **1:2**, 95-114.
- FEMA. 2012. Federal Emergency Management Agency P646, Guidelines for Design of Structures for Vertical Evacuation from Tsunamis, Washington, D.C., USA.
- FRITZ, H. M., PETROFF, C. M., CATALÁN, P. A., CIENFUEGOS, R., AND WINCKLER, P. (2011). Field survey of the 27 February 2010 Chile tsunami. *Pure and Applied Geophysics* **168:11**, 1989-2010.
- LAGOS, M., ARCAS, D., RAMIREZ, T., SEVERINO, R., AND GARCIA, C. (2010). Alturas de tsunami modelas y observadas. Evento del 27 de Febrero de 2010. Chile/Resultados Preliminares.
- NISTOR, I. (2012). Field survey of the tsunami impact and loading on structures – Engineering lessons of the 2011 Tohoku Tsunami. *4<sup>th</sup> International Conference on Protection of Structures against Hazards*.
- NISTOR, I., MURTY, T., NIRUPAMA, N., JINSONG, X. (2006). Some physical oceanographic processes in the behavior of the 26th December 2004 tsunami. *15<sup>th</sup> Congress of the Asia-Pacific Division of IAHR and International Symposium on Maritime Hydraulics, IAHR*, 81-90.
- NGDC. (2012). National Geophysical Data Center, National Oceanic and Atmospheric Administration. <http://www.ngdc.noaa.gov/hazard/recenttsunamis.shtml>.
- NOURI, Y., NISTOR, I., PALERMO, D., AND CORNETT, A. (2010). Experimental investigation of tsunami impact on free standing structures. *Coastal Engineering Journal, World Scientific* **52:1**, 43-70.

- PALERMO, D., NISTOR, I., SAATCIOGLU, M., AND GHOBARAH, A. (2013). Impact and damage to structures during the 27 February 2010 Chile tsunami. *Canadian Journal of Civil Engineering*, doi.org/10.1139/cjce-2012-0553.
- PALERMO, D., NISTOR, I., NOURI, Y., AND CORNETT, A. (2009). Tsunami loading of near-shoreline structures: A primer. *Canadian Journal of Civil Engineering* **36:11**, 1804-1815.
- SAATCIOGLU, M., GHOBARAH, A., AND NISTOR, I. (2006A). Performance of structures in Thailand during the 2004 Sumatra earthquake and tsunami. *Earthquake Spectra*, Earthquake Engineering Research Institute, **22:S3**, 355-376.
- SAATCIOGLU, M., GHOBARAH, A., AND NISTOR, I. (2006B). Performance of structures in Indonesia during the 2004 Sumatra earthquake and tsunami. *Earthquake Spectra*, Earthquake Engineering Research Institute, **22:S3**, 295-320.